IEICE TRANS. INF. & SYST., VOL.E102–D, NO.12 DECEMBER 2019

PAPER

A Fast Fabric Defect Detection Framework for Multi-Layer Convolutional Neural Network Based on Histogram Back-Projection

Guodong SUN[†a)], ***Member***, **Zhen ZHOU**[†], **Yuan GAO**[†], **Yun XU**[†], **Liang XU**[†], ***and*** **Song LIN**[†], ***Nonmembers***

SUMMARY In this paper we design a fast fabric defect detection framework (Fast-DDF) based on gray histogram back-projection, which adopts end to end multi-convoluted network model to realize defect classification. First, the back-projection image is established through the gray histogram on fabric image, and the closing operation and adaptive threshold segmentation method are performed to screen the impurity information and extract the defect regions. Then, the defect images segmented by the Fast-DDF are marked and normalized into the multi-layer convolutional neural network for training. Finally, in order to solve the problem of difficult adjustment of network model parameters and long training time, some strategies such as batch normalization of samples and network fine tuning are proposed. The experimental results on the TILDA database show that our method can deal with various defect types of textile fabrics. The average detection accuracy with a higher rate of 96.12% in the database of five different defects, and the single image detection speed only needs 0.72s.
key words: *back-projection, gray histogram, fabric detection, multi-layer convolutional neural network*

1. Introduction

In the textile industry, the presence of defects on the fabric reduces the value of the product, and the loss is as high as 45%-65% [1]. Therefore, the most important way to increase production efficiency and reduce production costs is to ensure the quality of fabric. However, for a long time, the detection of fabric defects has been done manually. There are many shortcomings, such as the low efficiency and high labour cost, and the human visual system can only identify about 50%-70% of textile fabrics [2]. Therefore, it is necessary to design an automatic detection method for fabric defects to reduce labour costs and improve fabric production efficiency. Currently, the textile industry divides fabric defects into more than 70 different categories [3]. Most of these defects are composed of holes, broken weft, oil spot, broken warp and breaking.

At present, the methods of fabric texture feature extraction are mainly divided into statistical methods, spectral methods and model methods [1]. Statistical methods mainly include gray level co-occurrence matrix (GLCM) [4], [5], fractal dimension [6], morphology [7] and Local binary pattern (LBP) [8]. Spectral methods include Fourier transform [9], Gabor filter [10], [11] and wavelet transform [12]. Model methods include autoregressive models and Markov fields [13]. On the other hand, some researchers use machine learning algorithms to incorporate defect classification into defect detection, making these algorithms more efficient. Zhang [14] optimizes neural network parameters by genetic algorithm and used Elman network model to classify fabric defects, which has better effect on different defect classification. Salem [2] compared several feature extraction methods and combined with support vector machine (SVM) to obtain better classification results, but such algorithm has low accuracy for different types of defects.

Although the above methods have some effects, their computational efficiency is not high. Back-projection is a method suitable for periodically detecting fabric defects in fabric textures. Swain et al. [15] first proposed a back-projection of color histogram based on target positioning. And a large number of subsequent researches also focused on the back-projection of color histogram [16]–[19]. Color histogram back-projection is mainly used for the detection and tracking of targets in complex backgrounds. It is necessary to know the color or region information of the target in advance. However, the fabric objects studied in this paper are mainly grey fabric, and there are many kinds of grey fabric defects. It is impossible to know what defects will occur before the detection, and there is no suitable color information, so the exact information of the defect cannot be provided. Therefore, we proposed a method based on gray histogram back-projection for fabric defect segmentation.

On the other hand, after AlexNet [20] was successful in image recognition tasks, some deep learning methods similar to convolutional neural networks (CNN), have set off a research boom in many computer vision tasks. Mei et al. [21] train multiple convolutional denoising autoencoder networks with randomly sampled image blocks from defect-free samples, and finally predict the defects by synthesizing multiple pyramid layers. However, in these visual recognition task, most researchers use a network detection model from coarse to fine. For example, Sun et al. [22] proposed a system for recognizing typical faults based on CNN, which can solve the problem of low quality images. The fault inspection system includes two complex models based on CNN, which are used for target region detection and faults recognition respectively, but their versatility and efficiency are not high. For an object detection tasks,

Manuscript received March 30, 2019.
Manuscript revised July 26, 2019.
Manuscript publicized August 26, 2019.
[†]The authors are with Hubei University of Technology, Wuhan, Hubei, China.
a) E-mail: sgdeagle@163.com
DOI: 10.1587/transinf.2019EDP7092

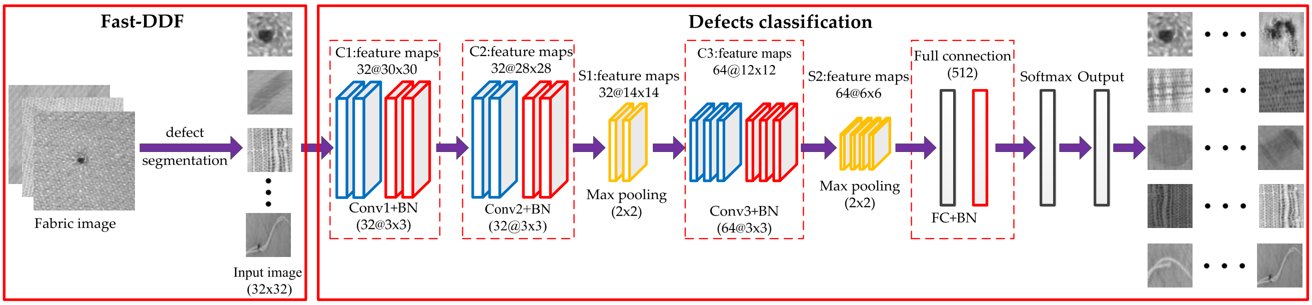

Fig. 1 Fast-DDF for multi-layer convolutional neural network based on gray histogram back-projection

region-based CNN (R-CNN) detection methods [23] such as Faster R-CNN [24] and the region-based fully convolutional networks (R-FCN) [25] are now main examples with increasingly better accuracy. However, the fabric image usually has a large size, and the defect only accounts for a small part of the whole image. If CNN is used for defect segmentation, it will take a lot of time.

As shown in Fig. 1, inspired by faster R-CNN, we design a fast fabric defect detection framework (Fast-DDF) for multi-layer CNN based on gray histogram back-projection. It consists of defect segmentation and defect classification. Defect segmentation is realized by a Fast-DDF based on gray histogram back projection. Since the gray histogram back-projection algorithm has the advantage of removing texture background information, we combine Adaptive threshold segmentation method to quickly extract fabric image defect region. Defect classification is achieved by designing an end-to-end multi-convolution network structure. We use sample batch normalization (BN) [26] and network finetuning strategies to improve network training efficiency.

The remainder of this paper is organized as follows. Section 2 presents the principles of the proposed fast fault detection framework. Section 3 introduces the construction of a multi-layer CNN. The databases, experimental results and analysis are shown in Sect. 4. We end this paper with the conclusion in Sect. 5.

2. Fast-DDF Based on Gray Histogram Back-Projection

2.1 Fast-DDF Process

The procedure of fabric defect detection is showed in Fig. 2. First, we calculate the gray histogram back-projection of the image, and then further remove the interference points in the back projection image by morphological processing. Further, the binarization processing and the defect connected operation are performed to obtain a complete defect region. Finally, locate the defect location in the original image.

2.2 Gray Histogram Back-Projection

The histogram back-projection based on pixels is to calculate the feature histogram of each pixel within the input image firstly, and then the character eigenvalue of each pixel in

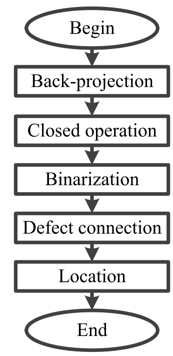

Fig. 2 Process of Fast-DDF.

input image should be replaced by the specific bin value to which the eigenvalue is corresponding in the histogram, and finally the back-projection image is obtained by the normalized result image. For example, in gray level images, the greater the number of the pixels with specific gray value is in the whole gray images, the greater its value is in the histogram, and the greater its corresponding value is in back-projection. Conversely, the smaller the region occupied by a certain gray value, the smaller its new value by back-projection is. The back-projection based on the gray histogram is shown as follows:

$$bp(i, j) = \frac{255 * q_{b(i,j)}}{\max(q_m)} \quad (m = 1, 2, \cdots n). \tag{1}$$

The $bp(i, j)$ is pixel value of back-projection in point (i, j). The $b(i, j)$ represents a bin of histogram to which the pixel at the point (i, j) corresponds. Histogram generally has n bins. The $q_{b(i,j)}$ is value of the bin $b(i, j)$. The q_m is value of the m-th bin in histogram. The $\max(q_m)$ means the max value of them.

In addition, because of the characteristics of fabric texture, the gray values of the defective pixels and non-defective pixels in the back projection are close to each other, which is difficult to distinguish. In order to detect defects more effectively, the calculation equation of back-projection can be changed as follows:

$$bp(i, j) = \begin{cases} q_{b(i,j)} & q_{b(i,j)} < 255 \\ 255 & q_{b(i,j)} \geq 255 \end{cases}. \tag{2}$$

After calculating image histogram, if the number of pixels corresponding to the gray value is less than 255, the number of pixels is taken as the gray value of these pixels. If the number of pixels corresponding to the gray value is greater than or equal to 255, the gray value of these pixels is set to 255. In this way, most of the non-defective pixels can be filtered out, and then back-projection of the rest pixels will be more targeted.

As shown in Fig. 3, the original, binarization and back-projection images are shown from left to right. The experimental results show that the pixel values in the fabric images have different levels from high to low, and gray values of pixels belonging to defects are also different, simple binarization processing may not separate defects out. However, the image will well retain defective regions after back-projection and eliminate non-defective regions through morphological processing. Regardless of directions of the fabric texture, back-projection has a great effect for shielding fabric texture. Compared with Gabor transform which need to determine directions of the texture or Gabor nucleus of multiple dimensions and scales, back-projection is practical and can greatly reduce the complexity.

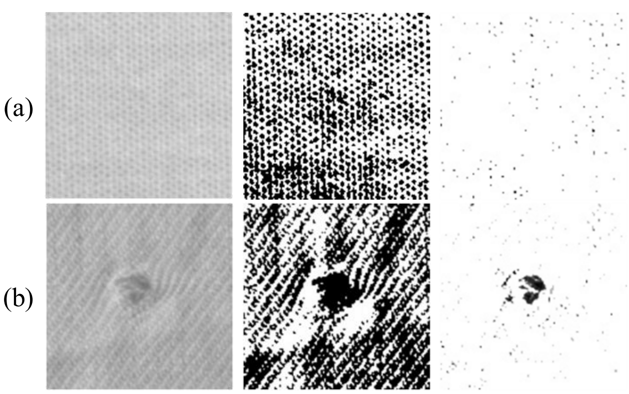

Fig. 3 Comparison of processing results with binarization and back-projection. (a) Images with no defects; (b) images with hole defects (from left to right are the original image, binarization image and back-projection image).

2.3 Parameter Selection for Back-Projection

When calculating the histogram of gray image of the fabric, the size of the histogram, that is, the number m of bins, has a certain influence on the back-projection image. Since there are 256 gray levels in the gray image, when m is equal to 16, each bin occupies 16 gray levels. If m is equal to 256, each gray level corresponds to one bin. Taking the fabric image with hole defects as an example, when m is equal to 8, 16, 32, 64, 128 and 256, the corresponding back-projection and final processing effect of the hole defects image are shown in Fig. 4.

From Fig. 4 (a), it can be seen that the average gray value of the region near the defect is significantly lower than other regions. With the increasing of m, impurities in back-projection will gradually aggrandize. But if m is too small, it can be seen from Fig. 4 (b) that regions of detected defects will shrink. So it is not conducive to help us find complete defect region.

In order to select the range of m reasonably. The probability of defects which may be detected in the back-projection image is denoted as A, and the possessive probability of defects in the back-projection image is denoted as B. The number of pixels belonging to hole defects in Fig. 3 (b) is Q. The amount of the pixels which are detected and belong to hole defects in Fig. 3 (b), is recorded as C. The amount of the pixels, whose corresponding number is less than 255 in the gray histogram of Fig. 3 (a), is recorded as P. The calculation formulas of A and B are as follows:

$$A = \frac{C}{Q};\ B = \frac{C}{P} \tag{3}$$

As shown in Fig. 5, A and B in the hole defect image with m ranging from 8 to 256 are counted. With the increase of m, A and B is fluctuant in local part due to uneven gray distribution of defects, but overall A increases and B decreases gradually. The greater A and B are, the better effect of defect detection is. But the tendency of A

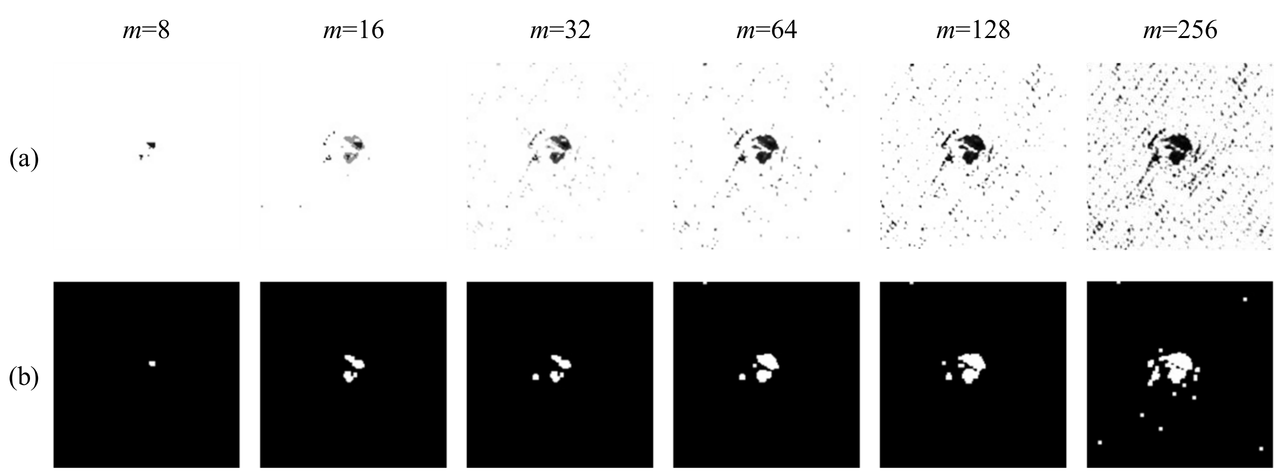

Fig. 4 Effect of bin values on back-projection: (a) back-projection image; (b) final result image.

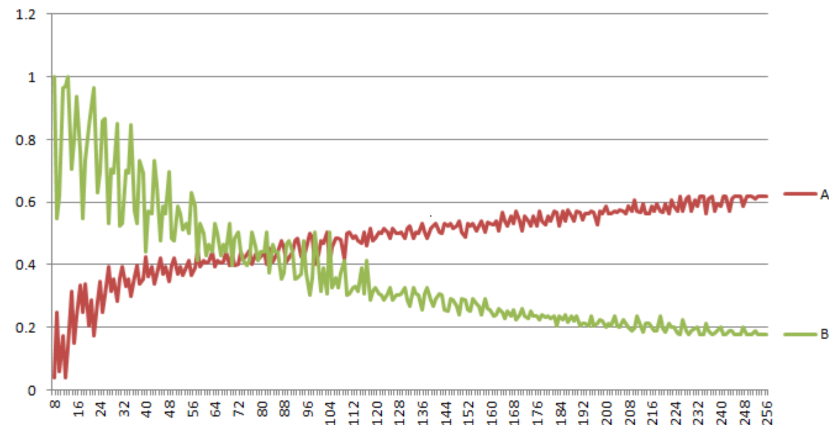

Fig. 5 A and B changing with m in the hole defect image.

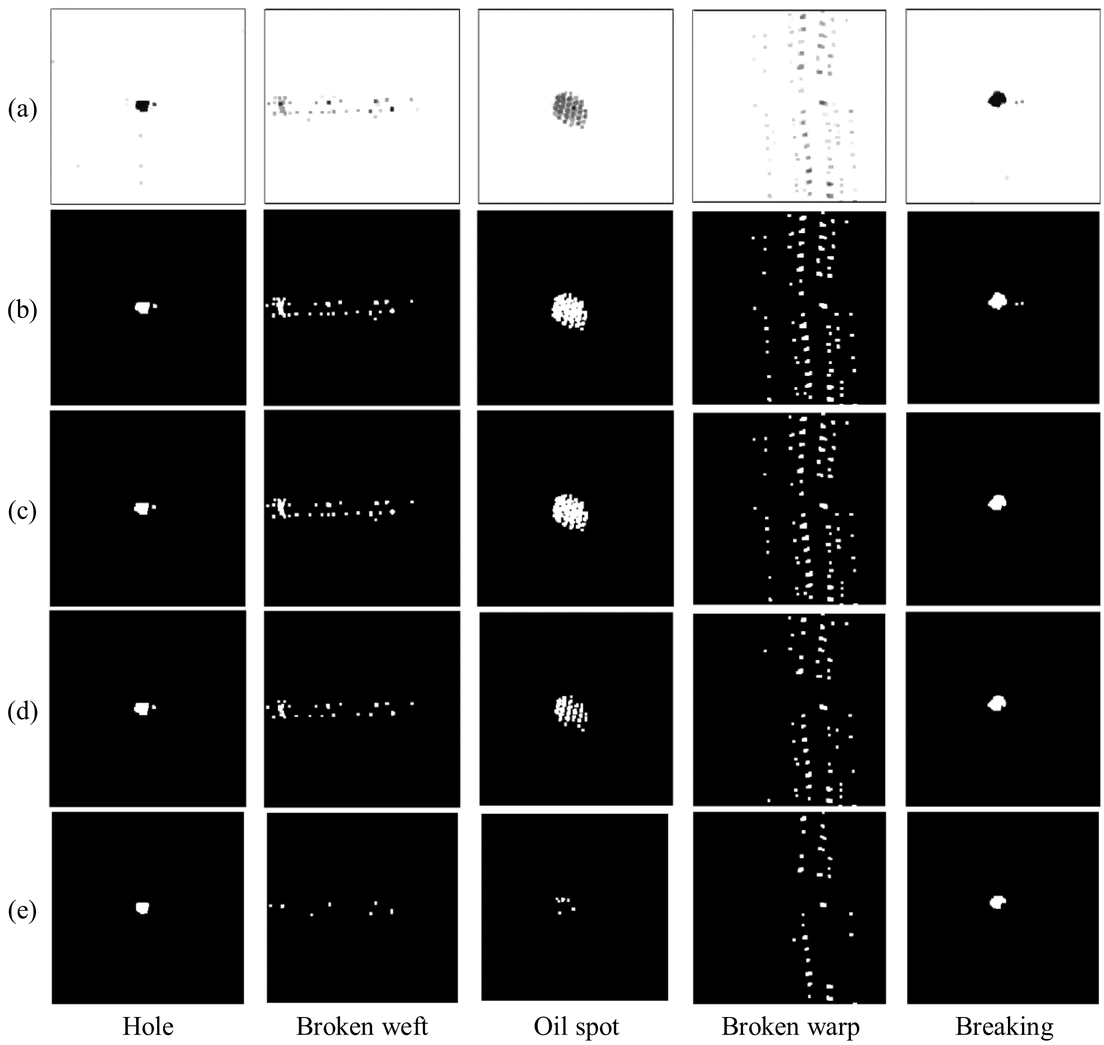

Fig. 6 Experimental results of different threshold segmentation methods. (a) Fabric defect images; (b) basic global threshold segmentation result; (c) Otsu segmentation result; (d) maximum entropy threshold segmentation result; (e) iterative segmentation result.

and B is opposite, so it is necessary to find a balance point. Smaller A or B is not desirable, so we performed experiments on multiple sets of images for each defect, and finally found that m has the best range from 56 to 104. Along with the change of defect types and light, it will change a little but does not deviate too far. However, it is impractical to

Table 1 Speed of different binarization methods for fabric defect images

Methods	Time(ms)					Average time(ms)
	Hole	Broken weft	Oil spot	Broken warp	Breaking	
Basic global threshold	6.21	8.27	7.43	7.15	5.32	6.88
Otsu	0.53	0.65	0.49	0.67	0.48	0.56
Maximum entropy threshold	126.67	129.82	128.26	148.05	118.14	130.19
Iteration method	0.27	0.58	0.35	0.44	0.37	0.40

manually select a different m for each image during fabric defects detection. Therefore, we can verify and select the empirical value first. As long as the value of m is feasible within the effective interval, m is set as 80 in this paper.

2.4 Morphology Processing

The morphology processing after back-projection is very important to avoid the interference of impurities. The location region where the defect is located will be retained, and no error will be judged for the image without the defect. The erosion of gray image is to select the minimum of the difference between image pixels and structural elements in neighborhood block determined by structural elements. The dilation of gray image is expressed as selecting the maximum of the sum between image pixels and structural elements in neighborhood block determined by structural elements. Structural element of 3×3 is adopted in this paper.

2.5 Binarization and Defect Connection

Since the image after the closed operation is a gray image, binarizing the image is advantageous for positioning the defect. According to the principle of back-projection, the pixel with high gray value has high occupancy rate after back-projection, so there are some independent small interference points after the closing operation. If the threshold of binarization is too small, the defect will also be filtered. In order to eliminate some of the interference points without excessively reducing the defect region, a suitable binarization threshold is required. Obviously, a fixed threshold is not suitable, so it is necessary to choose an adaptive threshold segmentation method. Since the image after the closed operation shows obvious foreground and background, there is a significant trough in the histogram. However, common adaptive threshold segmentation methods include basic global threshold segmentation method, maximum interclass variance (Otsu) segmentation method, maximum entropy threshold segmentation method and iterative segmentation method. We perform experiments on four methods, and the results are shown in the Fig. 6.

It can be seen from the experimental results in Fig. 6 that basic global threshold segmentation method, Otsu and maximum entropy threshold segmentation have effects, and the basic global threshold segmentation method and Otsu segmentation method have the best retention of the defects as a whole, so they have the best effect. From Table 1, it can be concluded that iteration segmentation method is the fastest, but its experimental results lose more information about defects. However, the speed of Otsu segmentation method is not lagging behind with iteration segmentation method. Therefore, we use Otsu segmentation method to perform binarization processing on the image. Most defects after binarization are discrete, and we connect defects into a whole through connected domain processing.

The contours of binarization image are marked as the defects by minimum bounding rectangle method. When solving minimum bounding rectangles of the contours, the contours with smaller region can be excluded according to the quality requirements of fabric. In addition, all the reserved contours in images can be judged as defects as long as they are located, thereby the location method could be more accurate and rapid.

3. Defect Classification Based on Multi-Layer Convolutional Neural Network

The classical CNN is mainly composed of multiple convolutional layers and pooling layers. It is widely used in image recognition because of its strong robustness to translation, scaling and deformation. The structure of CNN proposed in this paper for classification of fabric defect is shown in Fig. 1. It is mainly composed of three convolution layers, two pooling layers, one fully connected layer and one Softmax layer. The details will be described later in this section.

The first six layers of this network are used for the extraction of defect features, and the last layer is used for classification. The batch size of each layer is uniformly set to 128. The activation function adopts ReLu. The output layer adopts Softmax regression with strong nonlinear classification ability and fast speed as the classifier. The loss function adopts cross-entropy.

3.1 Batch Normalization

Network training is a complicated process. When a certain layer of data changes slightly, the changes of subsequent layers of changes will be cumulatively amplified, and the network needs to re-adjust the learning rate and other parameters to adapt to the new data distribution, further affecting the training speed and accuracy. The change of data distribution in the middle layer during the training process is called as "Internal Covariate Shift", and BN [26] is an effective method to solve this problem.

BN refers to normalizing the input data in units of batch samples in a random gradient descent, so that the probability distribution of each latitude becomes a stable probability distribution with a mean of 0 and a standard deviation of 1. In order to avoid the destruction of the features learned in the normalization, it is necessary to introduce two trainable parameter γ and β to transform and reconstruct the data. If the input of a layer is $x = (x^1, \cdots, x^d)$, the total dimension is d, the batch size is set to m, and the sample set of a batch is $B = \{x_1, \cdots, x_m\}$, then the BN can be defined as follows:

$$\mu_B = \frac{1}{m}\sum_{i=1}^{m} x_i \tag{4}$$

$$\sigma_B^2 = \frac{1}{m}\sum_{i=1}^{m}(x_i - \mu_B)^2 \tag{5}$$

$$\hat{x}^{(k)} = \frac{x^{(k)} - \mu_B}{\sigma_B} \tag{6}$$

$$y^{(k)} = \gamma^{(k)}\hat{x}^{(k)} + \beta^{(k)} \tag{7}$$

μ_B, σ_B^2 represent the mean and variance of the sample set B, respectively. The normalized result of input $x^{(k)}$ is $\hat{x}^{(k)}$, $y^{(k)}$ represents the result of linear transformation of $\hat{x}^{(k)}$. $\gamma^{(k)}$, $\beta^{(k)}$ represent the parameters to be learned corresponding to $x^{(k)}$. In the CNN, a feature map can be treated as a neuron for processing due to weight sharing. It means that the mean and variance of all the neurons of a feature map are obtained, and then the neurons of the feature map are normalized.

In the proposed network, the BN layer is placed in front of the activation function layer, and the calculation of forward conduction is as follows:

$$z = g(BN(W \times u + b)), \tag{8}$$

Where W and b are the layer weights and thresholds, $g(\cdot)$ is the activation function, u is the input of the BN layer, z is the output obtained of the activation function.

3.2 Parameter Optimization

In the convolutional neural network, the random gradient descent method based on small batch samples is usually used, but this method is difficult to select for suitable hyperparameters, and the selection of parameters such as learning rate and initial weight will affect training speed and classification effect to some extent. Therefore, the adaptive parameterization method is widely used in the model tuning of the network, and the Adam method [27] is one of the representatives. Its main idea is to dynamically adjust the learning rate of each parameter by using the first moment estimation and the second moment estimation of the gradient. The iterative learning rate will be used each time after the offset correction and it is limited to a certain range, so that the parameters are relatively stable and the training speed is accelerated. Its formula is as follows:

$$m_t = \beta_1 * m_{t-1} + (1 - \beta_1) * g_t, \tag{9}$$

$$n_t = \beta_2 * n_{t-1} + (1 - \beta_2) * g_t^2, \tag{10}$$

$$\hat{m}_t = \frac{m_t}{1 - \beta_1^t}, \tag{11}$$

$$\hat{n}_t = \frac{n_t}{1 - \beta_2^t}, \tag{12}$$

$$\Delta\theta_t = \frac{\hat{m}_t}{\sqrt{\hat{n}_t + \varepsilon}}\eta, \tag{13}$$

Where m_t and n_t are the first moment and the second moment estimate of the gradient g_t, respectively. β_1 and β_2 represent the corresponding exponential decay factor, and the value range is $[0, 1)$. $\hat{m}_t$ and $\hat{n}_t$ are the correction of m_t and n_t, respectively. $\Delta\theta_t$ represents the update amount of the parameter. η represents the learning rate. ε is the minimum value which is greater than 0.

The Adam method can adaptively adjust the network parameters to make the network converge quickly, but the final training results often fail to achieve optimal results. In this paper, a parameter training method combining Adam and traditional SGD is used. In the early stage, the Adam method is used to adaptively adjust the learning rate to make the network converge quickly. In the later stage, the SGD method is used to further fine-tune the trained model with a very small learning rate to achieve an optimal classification effect.

4. Experimental Results

The experimental database has a total of 1000 images containing two parts: the TILDA database [28] and the other part of our own database. This paper mainly focuses on five kinds of common defects such as holes, broken weft, oil stain, broken warp and broken joint in plain weave fabric. In the TILDA database, we select two types of plain weave fabric samples, C1 and C2. Each type of defect contains 50 sample images for a total of 500 images. In our own database, 100 images are selected for each type of defect, for a total of 500 images. All image sizes are normalized to 800×600 pixels. The experimental environment is as follows: Windows 10 (×64) operating system, CPU Intel Core I7-6700 v4 @2.60GHz and 16GB RAM, all experiments are implemented by Matlab and Tensorflow. Furthermore, in order to effectively verify the performance of the algorithm, four evaluation indicators are established [29]: correct detection rate (CDR), missing detection rate (MDR), false detection rate (FDR), and detection speed. For example, suppose the number of all fault images in the test set is n, the number of detected fault images is a, the number of undetected fault images is b, and the number of incorrect image detection results is c. So, the above indexes can be defined as: CDR $= a/n$, MDR $= b/n$, FDR $= c/n$.

4.1 Frame Experiment of Defect Extraction

Image block feature is an effective method for dimensionality reduction. Its effect is equivalent to compressing image,

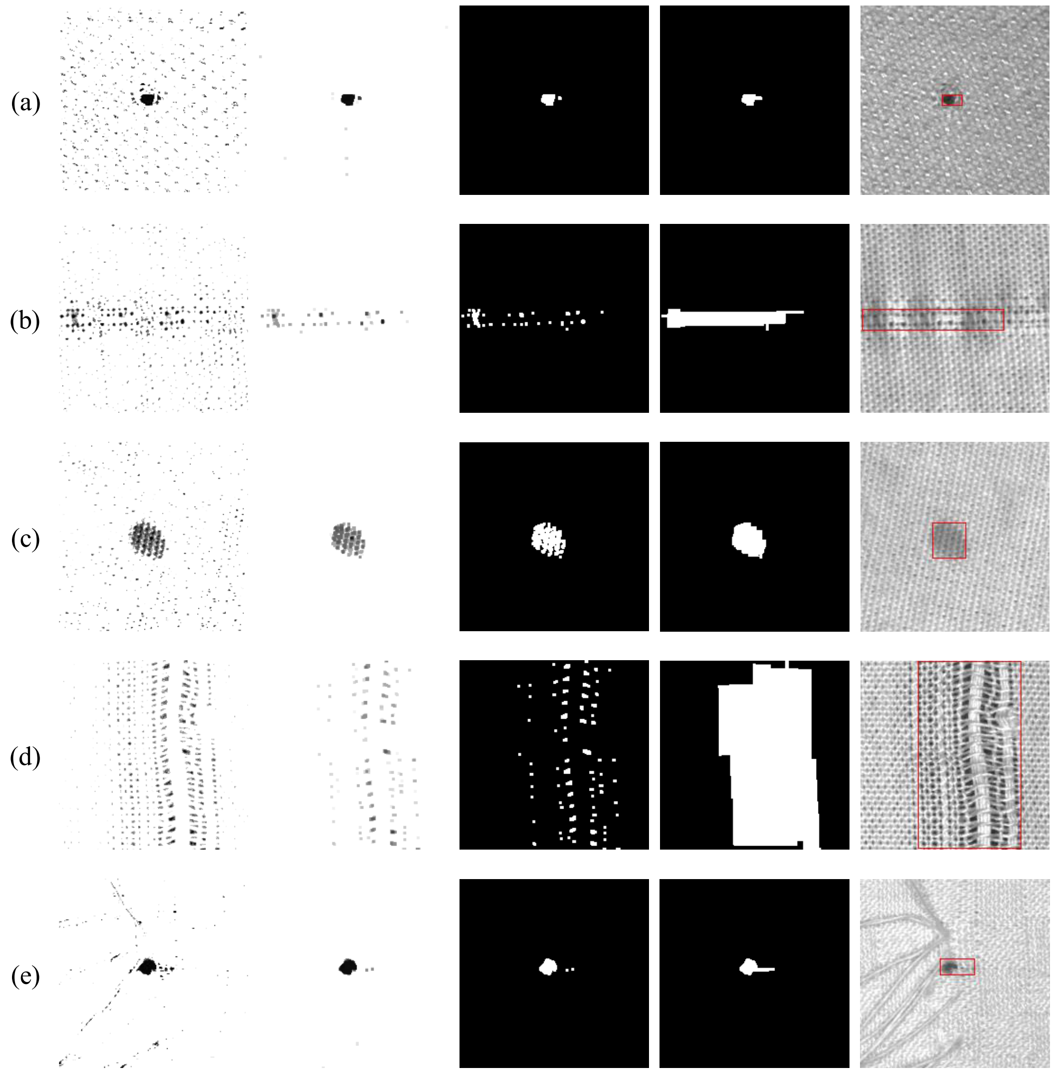

Fig. 7 Effect of partial defect detection: (a) hole; (b) broken weft; (c) oil spot; (d) broken warp; (e) breaking (from left to right are back-projection, closed operation, binarization, defect connection, result images).

reducing image resolution, and reducing the total histogram statistics when the histogram is projected backward. At the same time, by partitioning the sample image, mutual interference between multiple defects on the same image can be reduced to some extent, and the number of defects can be increased. We divided all 1000 images in the database into 200×200 pixel windows to get 12000 sample images. Then defect detection is carried out through the proposed defect framework. Some detection results are shown in Fig. 7, from left to right are gray histogram back-projection, closed operation, binarization, defect connection, result images.

In order to illustrate the effectiveness of Fast-DDF, we compared the current mainstream fabric defect detection methods. With some widely used defect detection methods such as Gabor filter, LBP, lattice segmentation assisted by Gabor filters (LSG) [11], GLCM [4] and Faster RCNN [24]. All of the above experiments were performed on Matlab, and the parameters of above all methods are all default values. The experimental results are shown in Table 2. The comprehensive performance on the CDR of Faster RCNN is better than other algorithms, but the method has higher hardware requirements. The detection speed is much slower than other algorithms in general hardware environments. However, our detection framework has an absolute advantage in speed. In addition, it can be seen that our detection framework also performs well in terms of average detection rate.

4.2 Classification Experiment

In order to train the network, we divided the 1000 images in the database into a training library with 800 images and a test library 200 images respectively. The selection principle ensures that the five defect types are equally distributed. Then we extract the defect images from the 800 images in the training library through the defect detection framework in Sect. 4.1. Due to the different sizes of defect regions, in

Table 2 Different methods of defect segmentation results and speed

Methods		Gabor filter	LBP	LSG	GLCM	Fast-DDF	Faster-RCNN
Hole	CDR/%	90.32	93.29	97.24	94.75	**99.28**	99.12
	MDR/%	3.42	1.67	1.32	2.32	**0.72**	0.88
	FDR/%	6.26	5.04	1.44	2.93	**0**	0
	Speed/ms	16.45	348.09	216.30	24.48	**4.25**	425.15
Broken weft	CDR/%	83.50	92.12	96.72	92.58	95.63	**97.38**
	MDR/%	6.21	3.48	2.26	2.53	3.12	**2.12**
	FDR/%	10.29	4.4	1.02	4.89	1.25	**0.50**
	Speed/ms	16.49	357.95	220.48	23.42	**5.32**	482.09
Oil spot	CDR/%	76.64	85.61	94.18	86.24	93.74	**95.30**
	MDR/%	10.78	7.43	3.90	3.06	**2.32**	3.66
	FDR/%	12.58	6.96	1.92	10.70	3.94	**1.04**
	Speed/ms	16.43	358.09	226.31	26.31	**4.09**	452.68
Broken warp	CDR/%	80.26	87.75	95.25	91.27	**97.30**	97.15
	MDR/%	7.28	4.25	**1.53**	2.43	2.15	2.52
	FDR/%	12.46	8.00	3.22	6.30	0.55	**0.33**
	Speed/ms	16.86	367.78	215.08	25.68	**3.85**	430.72
Breaking	CDR/%	89.03	90.23	94.32	92.04	96.12	**97.62**
	MDR/%	4.26	3.32	3.21	5.27	**1.26**	1.33
	FDR/%	6.71	6.45	2.47	2.69	2.62	**1.05**
	Speed/ms	16.02	338.43	206.82	22.45	**3.67**	452.30

Table 3 Comparison of network structure models

	A	B	C	D
network structure	Input image（32×32）			
	Conv1(32×3×3)	Conv1(32×3×3) BN	Conv1(32×3×3) BN	Conv1(32×3×3) BN
	Max pooling(2×2)	Max pooling(2×2)		
	Conv2(32×3×3)	Conv2(32×3×3) BN	Conv2(32×3×3) BN	Conv2(32×3×3) BN
	Max pooling(2×2)	Max pooling(2×2)	Max pooling(2×2)	Max pooling(2×2)
			Conv3(64×3×3) BN	Conv3(64×3×3) BN
			Max pooling(2×2)	Max pooling(2×2)
	FC (1×512)	FC (1×512) BN	FC (1×512) BN	FC(1×1024) BN
	Softmax			
Accuracy rate(%)	94.37	96.43	97.30	97.47
Detection time (s)	0.24	0.33	0.69	1.02

Table 4 Defect detection results of different methods.

Methods	CDR /%	MDR/%	FDR/%	Speed/s
LBP+BP-AdaBoost	94.86	1.83	3.31	1.07
LBP+AdaBoost+SVM	93.35	2.38	4.27	0.84
LBP+KNN	88.63	4.39	6.98	1.58
GLCM+BP	93.52	4.35	**2.13**	1.12
LSG+SVM	95.40	2.12	2.48	0.93
Fast-DDF+SVM	94.26	3.49	2.25	**0.58**
Our method	**96.12**	**1.20**	2.68	0.72

order to facilitate network training, all defect samples were normalized to 32 × 32 pixel images and marked, and the marked sample images were put into the network model for training.

As can be seen from the comparison between model A and model B in Table 3, although the detection time is not reduced after the addition of BN, the accuracy of model B is significantly improved, which indicates that BN is feasible to improve the model training effect. Similarly, comparing model B and model C, it can be found that after adding a layer of convolution, the accuracy and detection time increase. After increasing the number of fully connected layers in the model D, the accuracy rate has a small increase, but the time cost also increases. Therefore, Model C is adopted in this paper.

In order to prove the effectiveness of our method, we combined the trained network with Fast-FDD for a complete test experiment. We chose three defect detection methods that performed well in Sect. 4.1, such as GLCM, LSG, and LBP. Combine them with mainstream machine learning classification methods to compare experiments with our methods. With some widely used classification methods such as back propagation (BP), BP-AdaBoost, AdaBoost with a linear SVM classifier [30] and K-nearest neighbor (KNN). All of the above experiments were performed on Matlab, and the parameters of above all methods are all default values. The experimental results are shown in Table 4, we can see that our method has 96.12% correct detection rate, 1.2% missing detection rate, 2.68% false detection rate. The result has certain advantages over other methods. Furthermore, Fast-DDF combined with linear SVM method performs best in speed, but it is not as accurate as our method.

5. Conclusion

In this paper, a universal fast fabric defect detection framework, Fast-DDF, based on gray histogram back-projection has been proposed. We introduce Fast-DDF into our designed CNN and achieve satisfied results. Our detection framework is sensitive to texture features and can detect defect regions very quickly. For the extracted defect regions, we normalize and put them into the designed network for training. This innovative way greatly reduces the computational complexity of the network training and improves the detection speed. Finally, the experimental results show that our method has great advantages in comprehensive performance compared with the existing methods. The average detection accuracy with a higher rate of 96.12%, and the single image detection speed only needs 0.72s. Of course, this detection framework only has a good effect on the texture features. In the future, we will consider optimizing the framework structure and studying the application of CNN in texture defect segmentation, so that our framework has a larger application scenario.

Acknowledgments

This work is supported by a grant from the National Natural Sciences Foundation of China (Grant 51775177, Grant 51675166). In addition, the authors give particular thanks to the contributors to the Fabrics, TILDA databases.

References

[1] A. Kumar, "Computer-Vision-Based Fabric Defect Detection: A Survey," IEEE Trans. Ind. Electron., vol.55, no.1, pp.348–363, Jan. 2008. DOI:10.1109/TIE.1930.896476

[2] Y.B. Salem and S. Nasri, "Automatic recognition of woven fabrics based on texture and using SVM," Proc. Signal Image and Video Processing, vol.4, no.4, pp.429–434, Aug. 2009. DOI: https://doi.org/10.1007/s11760-009-0132-5

[3] H.Y.T. Ngan, G.K.H. Pang, and N.H.C. Yung, "Automated fabric defect detection—A review," Image and Vision Computing, vol.29, no.7, pp.442–458, June 2011. DOI: org/10.1016/j.imavis.2011.02.002

[4] J.L. Raheja, S. Kumar, and A. Chaudhary, "Fabric defect detection based on GLCM and Gabor filter: A comparison," Optik, vol.124, no.23, pp.6469–6474, Dec. 2013. DOI: org/10.1016/j.ijleo.2013.05.004

[5] G. Zhao and S.Y. Qin, "High-Precision Detection of Defects of Tire Texture Through X-ray Imaging Based on Local Inverse Difference Moment Features," Sensors, vol.18, no.8, p.2524, Aug. 2018. DOI: org/10.3390/s18082524

[6] H.-G. Bu, J. Wang, and X.-B. Huang, "Fabric defect detection based on multiple fractal features and support vector data description," Engineering Applications of Artificial Intelligence, vol.22, no.2, pp.224–235, March 2009. DOI: org/10.1016/j.engappai.2008.05.006

[7] K.L. Mak, P. Peng, and K.F.C. Yiu, "Fabric defect detection using morphological filters," Image and Vision Computing, vol.27, no.10, pp.1585–1592, Sept. 2009. DOI: org/10.1016/j.imavis.2009.03.007

[8] W.Y. Li, W.L. Xue, and L.D. Cheng, "Intelligent detection of defects of yarn-dyed fabrics by energy-based local binary patterns," Textile Research Journal, vol.82, no.19, pp.1960–1972, Nov. 2012. DOI: 10.1177/0040517512444332

[9] A.S. Malek, J.-Y. Drean, L. Bigue, and J.-F. Osselin, "Optimization of automated online fabric inspection by fast Fourier transform (FFT) and cross-correlation," Textile Research Journal, vol.83, no.3, pp.256–268, Feb. 2013. DOI: 10.1177/0040517512458340

[10] D.-C. Choi, Y.-J. Jeon, S.H. Kim, S. Moon, J.P. Yun, and S.W. Kim, "Detection of Pinholes in Steel Slabs Using Gabor Filter Combination and Morphological Features," Isij International, vol.57, no.6, pp.1045–1053, June 2017. DOI: 10.2355/isijinternational.ISIJINT-2016-160

[11] L. Jia, C. Chen, J.Z. Liang, and Z.J. Hou, "Fabric defect inspection based on lattice segmentation and Gabor filtering," Neurocomputing, vol.238, pp.84–102, May 2017. DOI: org/10.1016/j.neucom.2017.01.039

[12] G.-H. Hu, G.-H. Zhang, and Q.-H. Wang, "Automated defect detection in textured materials using wavelet-domain hidden Markov models," Optical Engineering, vol.53, no.9, pp.93–107, Sept. 2014. DOI: 10.1117/1.OE.53.9.093107

[13] Y. Zhang, G.M. Jiang, J.Z. Yao, and Y.C. Tong, "Intelligent segmentation of jacquard warp-knitted fabric using a multiresolution Markov random field with adaptive weighting in the wavelet domain," Textile Research Journal, vol.84, no.1, pp.28–39, Feb. 2013. DOI: 10.1177/0040517513485629

[14] Y.H. Zhang, C. Yuen, W.K. Wong, and C.-W. Kan, "An intelligent model for detecting and classifying color-textured fabric defects using genetic algorithms and the Elman neural network,"

Textile Research Journal, vol.81, no.17, pp.1772–1787, Oct. 2011. DOI: 10.1177/0040517511410102
[15] M.J. Swain and D.H. Ballard, "Indexing Via Color Histograms," International Journal of Computer Vision, vol.7, no.1, pp.11–32, Jan. 1991. DOI: 10.1109/ICCV.1990.139558
[16] F. Ennesser and G. Medioni, "Finding Waldo, or Focus of Attention Using Local Color Information," IEEE Trans. Pattern Anal. Mach. Intell., vol.17, no.8, pp.805–809, Sept. 1995. DOI: 10.1109/34.400571
[17] J.I. Agbinya and D. Rees, "Multi-Object Tracking in Video," Real-Time Imaging, vol.5, no.5, pp.295–304, Oct. 1999. DOI: org/10.1006/rtim.1998.0174
[18] J.-H. Lee, W.-H. Lee, and D.-S. Jeong, "Object tracking method using back-projection of multiple color histogram models," Proc. 2003 International Symposium on Circuits and Systems, vol.2, pp.25–28, May 2003. DOI: 10.1109/ISCAS.2003.1206062
[19] X.P. Chen, Q. Huang, P. Hu, M. Li, Y. Tian, and C. Li, "Rapid and precise object detection based on color histograms and adaptive bandwidth mean shift," Proc. International Conference on Intelligent Robots and Systems, IEEE, pp.4281–4286, Oct. 2009. DOI: 10.1109/IROS.2009.5354739
[20] A. Krizhevsky, I. Sutskever, and G.E. Hinton, "Image Net classification with deep convolutional neural networks," Proc. International Conference on Neural Information Processing Systems, vol.25, no.2, pp.1097–1105, Jan. 2012. DOI: 10.1145/3065386
[21] S. Mei, Y.D. Wang, and G.J. Wen, "Automatic Fabric Defect Detection with a Multi-Scale Convolutional Denoising Autoencoder Network Model," Sensors, vol.18, no.4, p.1064, April 2018. DOI: 10.3390/s18041064
[22] J.H. Sun, Z.W. Xiao, and Y.X. Xie, "Automatic multi-fault recognition in TFDS based on convolutional neural network," Neurocomputing, vol.222, no.26, pp.127–136, Jan. 2017. DOI: org/10.1016/j.neucom.2016.10.018
[23] G. Ross, D. Jeff, D. Trevor, and M. Jitendra, "Rich feature hierarchies for accurate object detection and semantic segmentation," Proc. Computer Vision and Pattern Recognition, pp.580–587, Oct. 2014.
[24] S.Q. Ren, K.M. He, R. Girshick, and J. Sun, "Faster R-CNN: towards real-time object detection with region proposal networks," IEEE Trans. Pattern Anal. Mach. Intell., vol.39, no.6, pp.1137–1149, June 2017. DOI: 10.1109/TPAMI.2016.2577031
[25] J.F. Dai, Y. Li, K.M. He, and J. Sun, "R-FCN: Object detection via region-based fully convolutional networks," Proc. Computer Vision and Pattern Recognition, May 2016.
[26] S. Ioffe and C. Szegedy, "Batch normalization: Accelerating deep network training by reducing internal covariate shift," Proc. Machine Learning, Feb. 2015.
[27] D. Kingma and J. Ba, "Adam: A method for stochastic optimization," Proc. Machine Learning, Jan. 2017.
[28] TILDA Database for Textile Defect Detection, Feb. 2017, available: http://lmb.informatik.uni-reiburg.de/research/dfg-texture/tilda
[29] G.D. Sun, Y. Zhang, H.B. Tang, H.M. Zhang, M.Y. Liu, and D.X. Zhao, "Railway equipment detection using exact height function shape descriptor based on fast adaptive Markov random field," Optical Engineering, vol.57, no.5, p.1, May 2018. DOI: 10.1117/1.OE.57.5.053114
[30] P. Dollar, R. Appel, S. Belongie, and P. Perona, "Fast Feature Pyramids for Object Detection," IEEE Trans. Pattern Anal. Mach. Intell., vol.36, no.8, pp.1532–1545, Aug. 2014. DOI: 10.1109/TPAMI.2014.2300479

Guodong Sun is a professor in the School of Mechanical Engineering at the Hubei University of Technology. He received his BS degree in energy and power engineering and his PhD degree in mechanical and electronic engineering from Huazhong University of Science and Technology in 2002 and 2008, respectively. His current research interests include machine vision and imaging processing.

Zhen Zhou received the B.S. degree from Hubei University of Technology, Wuhan, China, in 2015. He is currently pursuing the M.S. degree with the School of Mechanical Engineering, Hubei University of Technology, Wuhan, China. His current research interests are deep learning and imaging processing.

Yuan Gao received the B.S. degree from Hubei University of Technology, Wuhan, China, in 2018. She is currently pursuing the M.S. degree with the School of Mechanical Engineering, Hubei University of Technology, Wuhan, China. Her current research interests are machine learning and imaging processing.

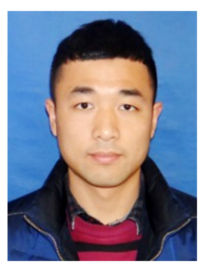

Yun Xu received the B.S. degree from Hubei University of Technology, Wuhan, China, in 2018. He is currently pursuing the M.S. degree with the School of Mechanical Engineering, Hubei University of Technology, Wuhan, China. His current research interests are machine learning and imaging processing.

Liang Xu received the B.S. degree from Hubei University of Technology, Wuhan, China, in 2017. He is currently pursuing the M.S. degree with the School of Mechanical Engineering, Hubei University of Technology, Wuhan, China. His current research interests are machine learning and imaging processing.

Song Lin received B.S. degree and M.S. degree from Hubei University of Technology, Wuhan, China, in 2012 and 2016, respectively. His current research interests include machine learning and imaging processing.